PHYSICAL REVIEW B VOLUME 46, NUMBER 7 15 AUGUST 1992-I

Molecular-dynamics study of single-electron charging in semiconductor wires

Kazuo Yano
Center for Solid-State Electronics Research, Arizona State University, Tempe, Arizona 85287
and Central Research Laboratory, Hitachi Ltd., Kokubunji, Tokyo 185, Japan

David K. Ferry
Center for Solid-State Electronics Research, Arizona State University, Tempe, Arizona 85287
(Received 24 February 1992)

A molecular-dynamics technique is applied to single-electron charging effects in semiconductor wires, and the impact of strong electron-electron correlation on the conductance is investigated. Because of the relatively low electron density in semiconductors compared to a metal, the screening length is comparable to the sample size, which requires a treatment beyond the conventional Coulomb-blockade argument using macroscopic capacitance. Based on the molecular-dynamics method, most features of the periodic conductance oscillation in the double-barrier system are reproduced, and the feasibility of this technique in single-electron charging phenomena is demonstrated. Experimental observation of an activation energy smaller than the threshold energy of the nonlinear conductance, which the normal Coulomb-blockade model cannot explain, is reproduced in the present approach. This effect is due to the strong microscopic correlation, so that this is essential to describe accurately the single-electron charging effects in semiconductor systems.

I. INTRODUCTION

Single-electron charging phenomena,[1,2] which cannot be accounted for without considering the quantization of charge, have recently attracted much attention. In metal tunnel junction systems, previously unreported physical phenomena, which include SET oscillation[3] and the Coulomb staircase,[4-6] have been found. Many experimental and theoretical efforts have been directed to the underlying physics of these phenomena. Single-electron charging phenomena are observed not only in metal systems but also semiconductors such as the Si-metal-oxide-semiconductor field-effect transistor[7] (MOSFET) and GaAs heterojunction two-dimensional electron gas (2 DEG) systems,[8-10] and insulators such as InO_2.[11] In metal tunnel junctions, the concept of Coulomb blockade and the "orthodox theory,"[1,2] which is a semiclassical treatment using macroscopic capacitances, charges, and potentials, have advanced the understanding of these phenomena by successfully explaining many observed results. These single-electron phenomena are thought to have tremendous possibilities in future electronics devices.[2]

However, in most experimental situations in semiconductors, the lack of several considerations in the conventional macroscopic approach restricts the applicability of this treatment to quantitative predictions. In the macroscopic model, the origin of a charge is the surface charge of an electrode, and the Coulomb energy is described in terms of the macroscopic capacitances. By contrast, in semiconductors the screening length of the electrons is comparable to, or even larger than, the device feature size. Therefore, estimating the Coulomb energy using a capacitance which is obtained simply from the sample geometry may lead to errors. In the macroscopic approach, the relaxation time in an electrode is neglected based upon the fact that an electrode contains a huge number of electrons. However, in semiconductors, the number of electrons in an "electrode" (or an isolated segment) is sometimes literally unity. We cannot neglect the relaxation time in such a situation. In the macroscopic approach, an electron is transferred instantaneously from one electrode to another and the transition time is neglected. Because barrier potentials are often smooth and continuous in semiconductors, the transfer is not limited to tunneling but may also be thermally activated, and metallic transfer is also important (the observed difference in the temperature dependence in two experiments[7,8] clearly shows the validity of this speculation). Therefore the transition time cannot be neglected. Based on this consideration, single-electron phenomena in semiconductors seem to be beyond the scope of the simple macroscopic capacitance approach. If one wants to stay with the macroscopic approach, the capacitance should be a complex function of the external frequency, the external wave vector, and the electron density. Moreover, if the Wigner crystallization of the electrons were to occur in the limit of strong electron correlation, the macroscopic capacitance approach is far away from the real system. These points suggest that an advanced approach, which can go beyond the macroscopic approach, is necessary for quantitative predictions.

One difficulty in the theory is providing a quantitative interpretation of experimental phenomena.[12,13] Although some aspects of the observed conductance oscillations in semiconductor wire structures can be explained by the Coulomb-blockade picture.[12,14,15] It has been suggested that there is a significant deviation when a quantitative

 ©1992 The American Physical Society

comparison is made.[13] The observed oscillations were first thought to be due to a charge-density wave (CDW) or Wigner crystallization of the electrons.[7,8] Later, it was suggested that the characteristics were explainable by the Coulomb-blockade model.[12] However, the observed activation energy is much less than that predicted by the Coulomb-blockade picture,[13] which raises a doubt about the current Coulomb-blockade interpretation in semiconductors.

The purpose of this paper is to gain insight into the above crucial question via numerical simulations. We use a classical molecular-dynamics technique so that the strong electron-electron correlations in a low-density regime and nontunneling-transfer mechanisms in smooth continuous potentials can be treated. The molecular-dynamics approach to electron transport[16,17] inherently incorporates the exact microscopic correlations, including multielectron scattering, without approximation (within the classical regime). It is also possible using this approach to discuss the impact of Wigner crystallization. The molecular-dynamics technique has been successfully employed to describe ultrafast optical-relaxation phenomena in semiconductors.[18,19] However, the applicability of this approach to single-electron charging phenomena has not been previously demonstrated, to the authors' knowledge. The molecular-dynamics approach will be described in Sec. II and the numerical results and discussion will be given in Sec. III.

II. MOLECULAR DYNAMICS

The system discussed is a semiconductor wire structure having a double-barrier potential, as shown in Fig. 1. It is known that, in a double-barrier system, single-electron charging effects are more easily observed than in the single-barrier counterpart, since a voltage-biased condition (without the need to provide constant current bias) can be used. Because of this, many experiments have been done in such double-junction systems. Figure 2 shows the external barrier potential that is imposed on the wire. This can be realized either by narrowing the effective wire width to raise the reference level of the potential or by introducing a bias through the presence of gate regions. Here we represent the potentials with a smooth analytical function, which decays as $\mathrm{sech}^2(2x/w_b)$, where w_b denotes the full width at half

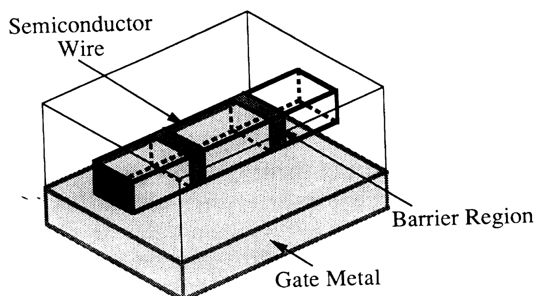

FIG. 1. Schematic of the wire structure and ground plane used in the simulation.

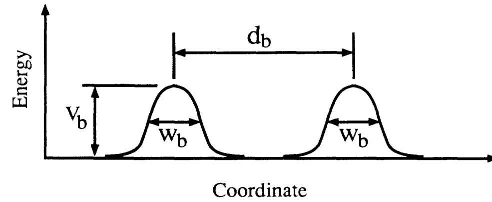

FIG. 2. Schematic view of the barrier potential and the parameters.

maximum of the barrier potential. The wire is assumed to be an undoped semiconductor, and the electron charge is neutralized by its image charge in the gate metal (or conductor). The spacing between the center of the wire and that of the image charge is assumed to 725 nm, which corresponds to the experimental condition of Ref. 9.

The molecular-dynamics technique is used to simulate the dynamics and statistical properties of the system. the electrons are modeled as a one-dimensional classical-particle system with mutual repulsion. The repulsive potential in our calculation includes the effect of the image charge in the metal, taking typical experimental conditions into account. The classical interelectron potential including this effect is

$$V_{e\text{-}e}=\frac{e^2}{r}-\frac{e^2}{\sqrt{r^2+d^2}}\ , \tag{1}$$

where e is the charge of an electron, r is the distance between two electrons, and d is the distance between the center of the electron and the center of its image charge. This potential is proportional to $1/r^3$ when $r \gg d$, corresponding to the repulsion between two dipoles.

Newton's equation of motion is discretized[20] as

$$x_i(t+\Delta t)=x_i(t)+\Delta t v_i(t)+(\Delta t)^2 F_i(t)/2\ , \tag{2}$$

$$v_i(t+\Delta t)=v_i(t)+(\Delta t)^2[F_i(t+\Delta t)+F_i(t)]/2\ , \tag{3}$$

where x_i and v_i denote the position and velocity of the ith electron, Δt denotes the time mesh, and F_i denotes the force upon the ith electron. The time evolution of this equation is simulated numerically and a statistical average is obtained by using the time average. This scheme neglects the influence of Fermi-Dirac statistics. However, in the range of electron density concerned, the Fermi level is small compared with the average Coulomb potential, which justifies this classical approximation. In fact, we are interested in a system which has the average interelectron distance larger than the effective Bohr radius in GaAs ($\sim$10 nm), which corresponds to the system having a linear density below 10^6/cm. Although the tunneling and interference effects are neglected in this approximation, the particle dynamics aspects of the electrons are clearly extracted in this simulation.

The conductance of the wire and the current are calculated by applying a voltage between the source and drain electrodes and counting the average electron flow. We do not use the conventional scheme that arises from use of the Kubo formula, mainly because we are interested in

the nonlinear conductance of the system. To avoid the (source and drain) edge effects, periodic boundary conditions are adopted. Electrons which pass the exit boundary lose their velocity information (they are assumed to equilibrate in the contact) and a particle is injected with a new velocity set to a random variable determined from a Maxwell distribution. The temperature of the system is maintained constant by using a velocity scaling technique.[20] The time mesh interval is determined so that energy conservation remains valid, without scattering at the boundary. Typically, a 100-fs interval is used in this simulation. The time average of a physical quantity is calculated using a stochastic sample typically over 10–30 ps. The temperature and the source-drain voltage can in principle be set to any arbitrary value. However, to have good convergence in realistic computation time, they cannot be too small. We typically use a temperature above 0.1 K and a drain voltage above 50 μV.

III. NUMERICAL RESULTS AND DISCUSSION

Using the above scheme, the current and the conductance of a single quantum wire, having double barriers, are investigated numerically. In Figs. 3(a)–3(c) we show the simulated conductance for different lengths of the isolated segment (or distance between the two barriers). Clear conductance oscillations are observed with increasing electron density. The significant conductance oscillations in Fig. 3, and their dramatically nonlinear characteristics, are remarkable when we recall that the results are derived by simply putting classical particles into a completely smooth potential, and are not obtained by quantization effects directly. We can clearly identify that it is the barrier potential which causes this oscillation, by noting that the oscillation disappears when the barrier potential is removed as shown in Fig. 3(d). We can relate this oscillation to the addition of a single electron to the isolated segment by simple calculations. We note the oscillation period is inversely proportional to the length of the isolated segment. This also shows that the oscillation corresponds approximately to the addition of a single electron to the isolated segment. This conclusion is more directly confirmed by the simulated average number of electrons in the segment $N_{\rm iso}$ shown in Fig. 4. The number of electrons increases exactly corresponding to the number of peaks in the conductance except for some offset integers. The conductance peak is revealed to correspond to the steep rise in $N_{\rm iso}$, whereas the conductance valley corresponds to a plateau in $N_{\rm iso}$ (although it is not always completely flat). This stepwise structure in the $N_{\rm iso}$ vs N curve (or the $N_{\rm iso}$ vs V_{gs} curve) is suggested in Ref. 15 in the context of the Coulomb blockade in a double-barrier semiconductor tunneling structure. Our numerical analysis shows that this property is also maintained in the continuous nontunneling regime. Although Figs. 3 and 4 take the carrier concentration as the horizontal axis, the horizontal axis can be as easily interpreted as the gate voltage. Because the distance between the real charge and the image charge is set to the same value as in Ref. 9, the electron-density increment of 1×10^4/cm can be interpreted as a gate voltage change of 0.475 mV.

It is worth noting that the conductance vanishes as the density drops to quite low values. There is also an indication in Fig. 3 that the conductance vanishes at higher densities, although this is not a density-dependent quantity, as can be seen by comparing the different lengths of the isolated region. This "vanishing" at higher densities is actually a region of low conductance, with the conductance again rising at higher values of the density, and is thought to be related both to the plateaus that arise in Fig. 4 and to the fact that the Coulomb energy of the par-

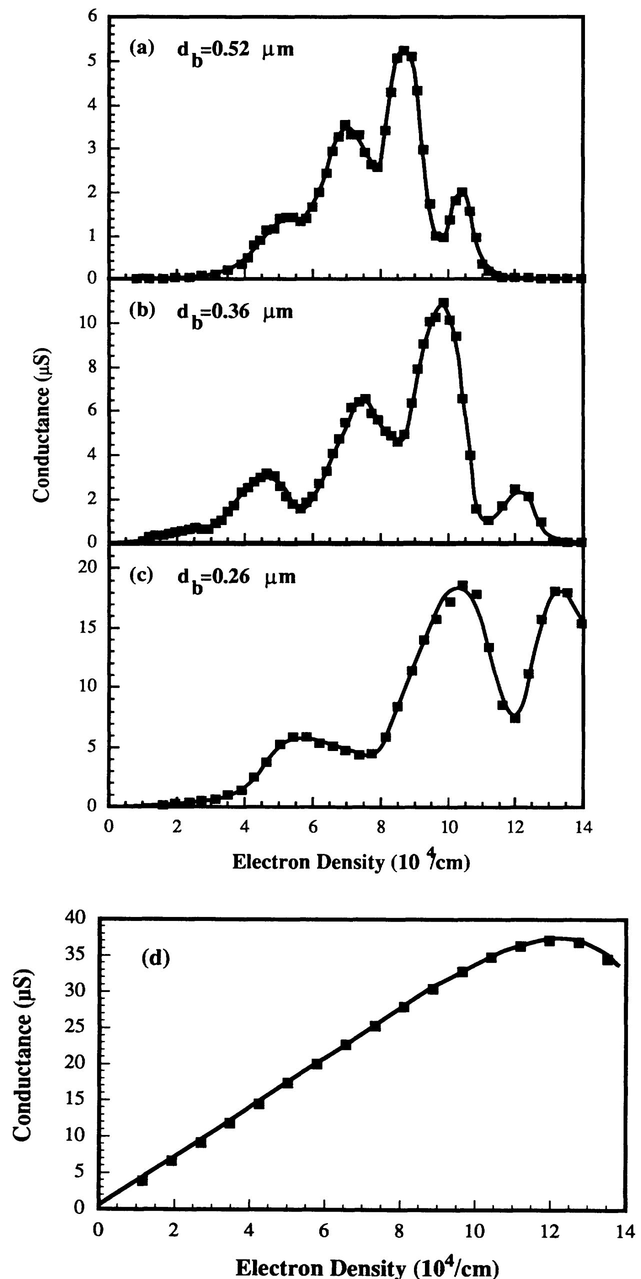

FIG. 3. Conductance as a function of the electron density for different lengths of the isolated segment d_b. The temperature is 0.37 K. The barrier height and the barrier width are 0.14 meV and 26 nm, respectively. The source-drain voltage is 425 μV. (d) shows the conductance in the absence of the barrier.

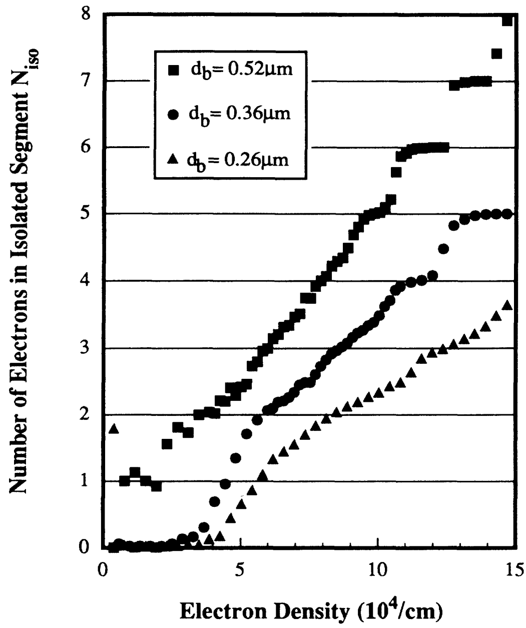

FIG. 4. The average number of electrons in the isolated segment between barriers as a function of the electron density for the conditions shown in Fig. 3.

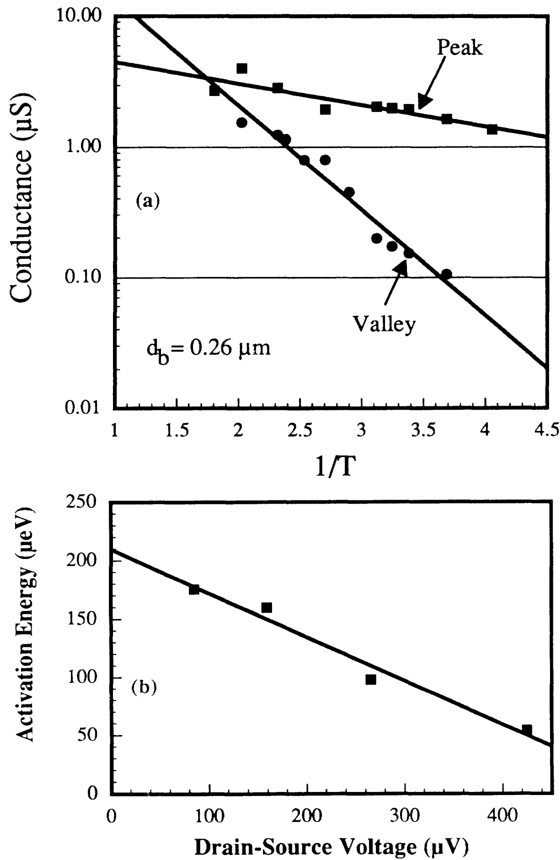

FIG. 5. (a) Arrhenius plot showing the temperature dependence of the conductance, at a maximum and at a minimum, of an oscillation. The drain-source voltage is 159 μV. (b) The dependence of the activation energy on the source-drain voltage.

ticles in the isolated region is significant as these electrons are compressed together. This effect is not fully understood, and will be the subject of further work.

The temperature dependence of the conductance is characterized by a single activation energy at low temperatures, as shown in Fig. 5(a). There is a difference in the activation energy between the peak values of the conductance and the local minima values of the conductance. Because of this, the oscillation almost disappears around 1 K in our simulations. To exclude the influence of finite source-drain voltage on the activation energy, we simulate the dependence of the activation energy on drain voltage and extrapolate to the zero-voltage condition as shown in Fig. 5(b). The activation energy is found to be 210 μV for the conditions of Fig. 3(a). Figure 6(a) shows dependence of the current on the source-drain voltage. When the gate voltage is set to a local minimum of the conductance, the current-voltage curve has a clearly nonlinear characteristic with a threshold voltage. The threshold voltage increases with a decrease in temperature, as shown in Figs. 6(a) and 6(b), and, at 0.185 K, it is 410 μV.

Despite the apparent limitation of the present approach in neglecting tunneling effects, the simulation reproduces many experimentally observed phenomena in quasi-one-dimensional semiconductor wires. First, the observed conductance oscillation corresponding to the addition of a single electron basically reproduces experi-

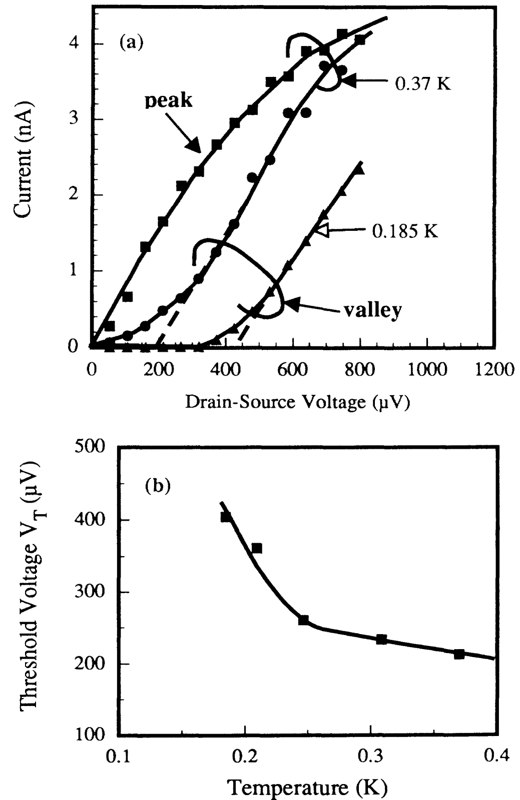

FIG. 6. (a) Current as a function of the source-drain voltage at the maximum and at the minimum of an oscillation. $d_b = 0.26\ \mu$m. (b) The threshold voltage vs temperature.

mental results.[7–9] The present simulation shows that the period of the oscillation is inversely proportional to the length of the isolated segment, which is what is seen in the experiment.[9] Because the absolute values of experimental conductances are reported to be subject to change after temperature cycling,[7–9] which indicates that the microscopic impurity configuration is affecting the results, the experimental conditions are not well characterized in this respect. However, the simulated peak conductances of 1–20 μS are close to experimental values of 1–12 μS (Ref. 9) and 1–15 μS.[8] The linewidth of each resonance in both the simulation and the experiment[9] is inversely proportional to the isolated-segment length.

The simulated activation energy E_a, which is smaller than the energy of the threshold voltage eV_T, needs special attention. The activation energy measured in the first experiment in a Si-MOSFET by Scott-Thomas *et al.*[7] was 50 μeV, whereas the eV_T was 200 μeV. In a subsequent experiment in a GaAs 2DEG structure by Meirav *et al.*,[8] the activation energy was 150 μeV and the threshold voltage energy was about 500 μeV. Both experiments show that the activation energies are smaller than the threshold voltage energies. Our simulation not only shows quite reasonable agreement in the absolute value of E_a (210 μeV) and V_T (410 μeV), but also agrees on the relative magnitudes of the two quantities. By contrast, the conventional Coulomb-blockade model for a double-junction system cannot predict this discrepancy between E_a and V_T.

Based on this agreement between the simulation and experiments, we expect that our model at least captures the essence of the observed phenomena. The early conjecture by Scott-Thomas *et al.*[7] of a pinned charge-density wave, and the Coulomb-blockade picture proposed by Van Houten and Beenaker,[12] are both models based on the competition between the barrier potential and the Coulomb potential. These are not mutually exclusive ideas. The former starts from an extended state over the entire electrode and the Coulomb energy is included by a macroscopic expression using the capacitance as $e^2/2C$. The latter starts from the ordered state in the strongly correlated limit and the Coulomb interaction is included as a microscopic expression as $e^2/4\pi\epsilon r$. The present analysis shows that the conductance oscillation occurs even without Wigner crystallization, but there is a tendency for ordering in the electron population. This is seen in the radial-distribution function shown in Figs. 7(a)–7(d) (we continue to use the common term radial-distribution function, although we clearly treat a linear correlation here). Although no crystallization is found in Fig. 7(b) at an electron density of 3.86×10^4/cm, the condition shown in Fig. 7(b) is beyond the scope of simple macroscopic capacitance arguments, because there is a strong correlation evident in the radial-distribution function. The total length scale corresponds roughly to the screening length of the electron system, and is comparable to, or larger than, the length of the isolated segment. The evident microscopic deviation from the smooth situation assumed in a macroscopic capacitance argument explains the observed deviation of the activation energy

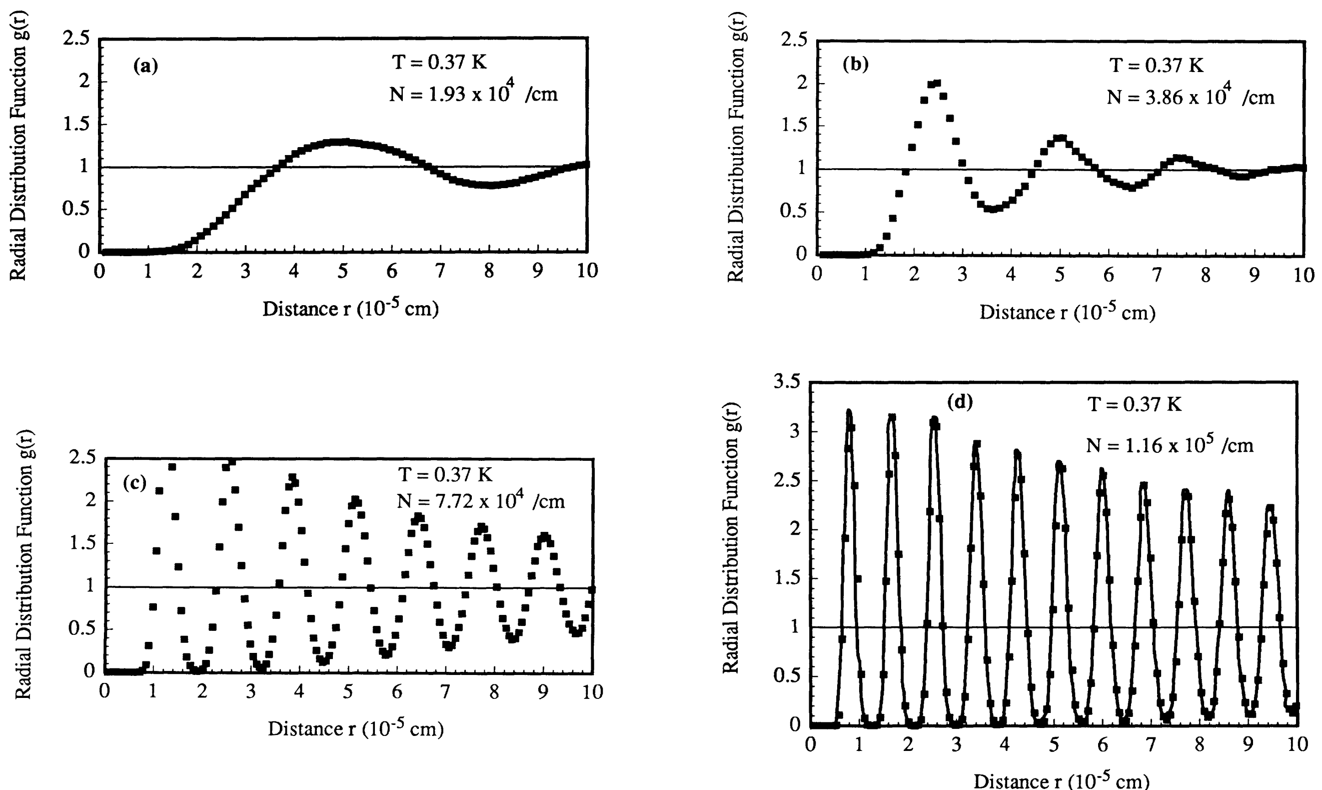

FIG. 7. Radial distribution function for different electron densities.

and the threshold energy from the macroscopic analysis.

The close relationship between the medium- to long-range correlation, and the large threshold voltage, is seen in the temperature dependence of the radial-distribution function shown in Fig. 8. At a density of 7.72×10^4/cm, strong correlation extending beyond the length of the isolated segment occurs roughly at 0.2–0.3 K. When we reexamine the temperature dependence of the threshold voltage in Fig. 6(b), we can clearly see a stronger temperature dependence below; such a temperature makes the threshold voltage much larger than the activation energy.

It should be noted that all the above results are obtained purely classically, without any quantum effect except charge quantization. This provides numerical evidence that a significant single-electron charging effect occurs in a completely smooth potential with a continuous-time electron transfer, even in the absence of tunneling. The fact that Coulomb-blockade affects may even be observed in a smooth potential without tunneling implies a significant impact not only on a fundamental understanding of the single-electron effects, but also on the application of such single-electronics concepts to future electron devices. Because an electron, in principle, can exist in any arbitrary position in a smooth potential, the basic argument of the Coulomb blockade (that the electron transfer inevitably increases the total energy, because only the discrete change of the electron state is allowed) fails. Likharev suggested in his review article[2] that the essence of his orthodox theory can possibly be applied to such a nontunneling-transfer process with metallic conduction, when the conductance of the junction is smaller than the quantum conductance unit $4e^2/h$. If we have a single-electron effect in such a nontunneling continuous electron transfer, the variety of systems which show these effects is drastically extended. Actually, the operating principle of current commercial transistors, such as a MOSFET, a bipolar junction transistor, or a high electron mobility transistor, is based on nontunneling thermal electron transfers. Therefore, these devices, when downscaled further, will possibly be affected by such single-electron charging. This will have an impact on the future applications of this concept.

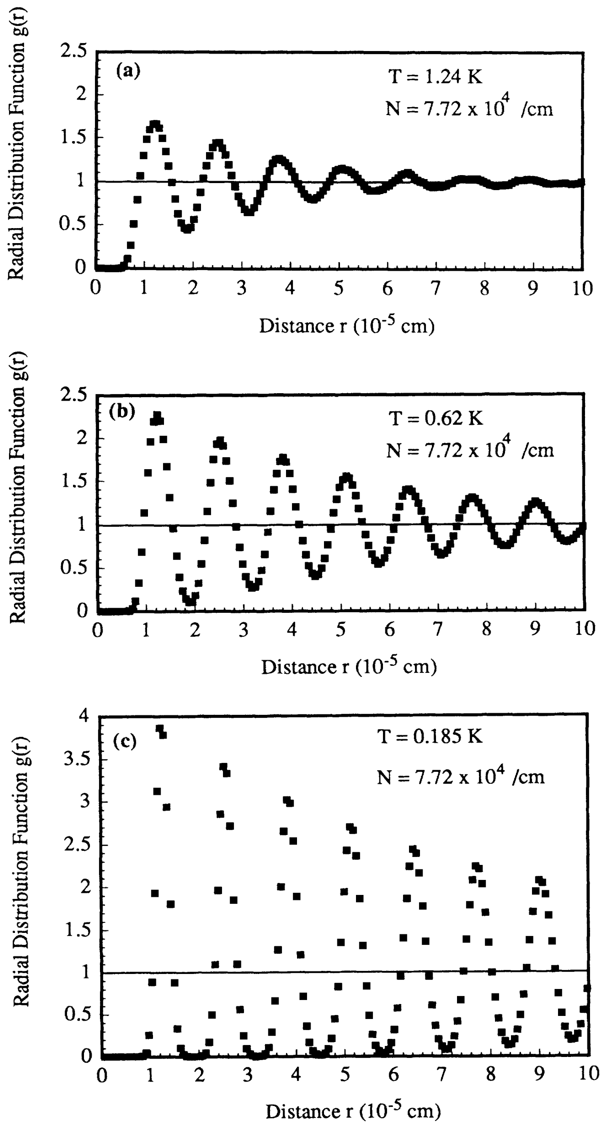

FIG. 8. Radial distribution function for different temperatures.

The characteristics of the downscaled (or upscaled) system from the system simulated above can be predicted without numerical simulations by using the following scaling property of the classical Newton's equation:

$$x'=\alpha x,\quad t'=\alpha^{1.5}t,\quad V_b'=V_b/\alpha\ ,$$

$$T'=T/\alpha,\quad I'=I/\alpha^{1.5}\ ,$$

where α denotes the scaling parameter, x denotes any coordinate such as the particle position and the barrier position, T denotes the temperature, and I denotes the current. The primed quantities represent the new scaled quantities. For example, if the size is downscaled by a factor of 2, while the potential barrier height and the temperature are upscaled by a similar factor, the current is larger than the original current by a factor of $2^{3/2}$. The peak-to-valley ratio of the conductance oscillation is unchanged by this transformation. Of course, in a drastically downscaled system the present fully classical approximation fails. However, it may still be valuable to know that such classical results distinguish the charging effects even in such a regime.

IV. CONCLUSION

The single-electron charging phenomenon in low-electron-density semiconductor wires is numerically analyzed by using a molecular-dynamics technique and incorporating microscopic electron correlation without approximation. This approach successfully reproduces the experimentally observed conductance oscillations, activation energy, and threshold voltage of the nonlinear conductance of a classical double-barrier structure. The present approach eliminates many discrepancies of the so-called orthodox model, and the oscillation is identified to be closely related to the medium- to long-range electron correlation (in the extreme case, Wigner crystalliza-

tion). The simulation also gives numerical evidence that significant single-electron charging effects can be observed in continuous, smooth potentials even without tunneling. This opens the door to a wide variety of single-electron effects in conventional semiconductor devices.

ACKNOWLEDGMENTS

The authors would like to thank Toshishige Yamada, Dr. Qin Li, Dr. Yukihiro Takagaki, and Fumiko Yano for useful discussions. Part of this work (D.K.F.) was supported by the Office of Naval Research.

[1]See, e.g., D. V. Averin and K. K. Likharev, in *Quantum Effects in Small Disordered Systems,* edited by B. Al'tshuler *et al.* (Elsevier, Amsterdam, 1991).

[2]See also *Granular Nanoelectronics,* edited by D. K. Ferry, J. R. Barker, and C. Jacoboni (Plenum, New York, 1991), particularly the articles by K. K. Likharev and L. J. Geerligs.

[3]D. V. Averin and K. K. Likharev, in *SQUID '85,* edited by H.-D. Hahlbohm and H. Lübiig (de Gruyter, Berlin, 1985), p. 197.

[4]T. A. Fulton and D. J. Dolan, Phys. Rev. Lett. **59**, 109 (1987).

[5]R. Wilkins, E. Ben-Jacob, and R. C. Jaklevic, Phys. Rev. Lett. **63**, 801 (1989).

[6]K. K. Likharev, IEEE Trans. Magn. **23**, 1142 (1987).

[7]J. H. F. Scott-Thomas, S. B. Field, M. A. Kastner, H. I. Smith, and D. A. Antoniadis, Phys. Rev. Lett. **62**, 583 (1989).

[8]U. Meirav, M. A. Kastner, M. Heiblum, and S. J. Wind, Phys. Rev. B **40**, 5871 (1989).

[9]U. Meirav, M. A. Kastner, and S. J. Wind, Phys. Rev. Lett. **65**, 771 (1990).

[10]P. L. McEuen, E. B. Foxman, U. Meirav, M. A. Kastner, Y. Meir, N. Wingreen, and S. J. Wind, Phys. Rev. Lett. **66**, 1926 (1991).

[11]V. Chandrsekhar, Z. Ovadyahu, and R. A. Webb, Phys. Rev. Lett. **67**, 2862 (1991).

[12]H. van Houten and C. W. J. Beenakker, Phys. Rev. Lett. **63**, 1893 (1989).

[13]M. A. Kastner, S. B. Field, U. Meirav, J. H. F. Scott-Thomas, H. I. Smith, and D. A. Antoniadis, Phys. Rev. Lett. **63**, 1894 (1989).

[14]M. Amman, K. Mulen, and E. Ben-Jacob, J. Appl. Phys. **65**, 339 (1989).

[15]L. I. Glazman and R. I. Shekhter, J. Phys. Condens. Matter **1**, 5811 (1989).

[16]P. Lugli and D. K. Ferry, Phys. Rev. Lett. **56**, 1295 (1986).

[17]D. K. Ferry, A. M. Kriman, M. J. Kann, and R. P. Joshi, Comp. Phys. Commun. **67**, 119 (1991).

[18]M. J. Kann, A. M. Kriman, and D. K. Ferry, Phys. Rev. B **41**, 12 659 (1990).

[19]P. Lugli, C. Jacoboni, L. Reggiani, and P. Kocevar, Appl. Phys. Lett. **50**, 1251 (1987).

[20]See, e.g., D. W. Heermann, *Computer Simulation Methods in Theoretical Physics* (Springer-Verlag, Berlin, 1990).

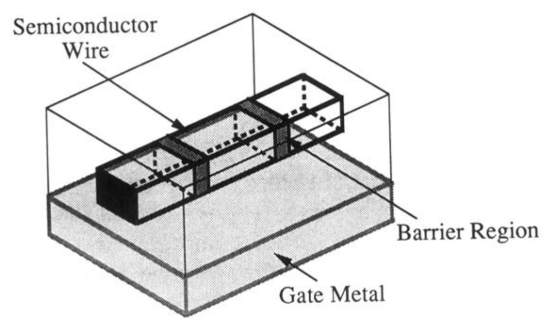

FIG. 1. Schematic of the wire structure and ground plane used in the simulation.